

# Bayesian Methods for the Investigation of Temperature-Dependence in Conductivity

Andrew R. McCluskey,<sup>1,2,\*</sup> Samuel W. Coles,<sup>3,4</sup> and Benjamin J. Morgan<sup>5,6</sup>

<sup>1</sup>*Centre for Computational Chemistry, School of Chemistry,  
University of Bristol, Cantock's Close, Bristol, BS8 1TS, UK.*

<sup>2</sup>*Diamond Light Source, Harwell Campus, Didcot, OX11 0DE, UK.*

<sup>3</sup>*Yusuf Hamied Department of Chemistry, University of Cambridge, Lensfield Road, Cambridge, CB2 1EW, UK.*

<sup>4</sup>*Lennard-Jones Centre, University of Cambridge, Trinity Lane, Cambridge, CB2 1TN, UK.*

<sup>5</sup>*Department of Chemistry, University of Bath, Claverton Down, Bath, BA2 7AY, UK.*

<sup>6</sup>*The Faraday Institution, Quad One, Harwell Science and Innovation Campus, Didcot, OX11 0RA, UK.<sup>†</sup>*

Temperature-dependent transport data, including diffusion coefficients and ionic conductivities, are routinely analysed by fitting empirical models such as the Arrhenius equation. These fitted models yield parameters such as the activation energy, and can be used to extrapolate to temperatures outside the measured range. Researchers frequently face challenges in this analysis: quantifying the uncertainty of fitted parameters, assessing whether the data quality is sufficient to support a particular empirical model, and using these models to predict behaviour at extrapolated temperatures. Bayesian methods offer a coherent framework that addresses all of these challenges. This tutorial introduces the use of Bayesian methods for analysing temperature-dependent transport data, covering parameter estimation, model selection, and extrapolation with uncertainty propagation, with illustrative examples from molecular dynamics simulations of superionic materials.

## I. INTRODUCTION

Transport coefficients, such as the self-diffusion coefficient  $D^*$  and ionic conductivity  $\sigma$ , are critical parameters for characterising the performance of technologies such as batteries, fuel cells, and memristors. These coefficients can be measured experimentally, for example, using impedance spectroscopy [1] or quasi-elastic neutron scattering [2, 3], or computationally from molecular dynamics or kinetic Monte Carlo simulations [4–7].

Transport coefficients are typically temperature dependent, with this temperature dependence commonly described by fitting empirical models to the measured data. Fitting offers a variety of benefits over presenting raw data alone. These benefits may be qualitative, such as the interpolation of a smooth, fitted curve to reveal trends obscured in raw data, or quantitative, such as allowing the transport coefficient to be predicted outside the measured regime, or providing fitted parameters (e.g., activation energies) that can be used to compare different materials. Fitted parameters may also connect to microscopic models of transport—for example, in solid ion-conductors, the activation energy is often interpreted as an approximation of the microscopic energy barrier for ion hopping [8, 9].

The most widely used empirical model for describing the temperature dependence of transport coefficients is the Arrhenius model. For diffusion, this takes the form

$$D^* = A \exp\left(\frac{-E_a}{RT}\right), \quad (1)$$

where  $E_a$  is the activation energy and  $A$  is the pre-exponential factor. For conductivity, the relationship between  $\sigma$  and  $D^*$  includes a  $T^{-1}$  term (from the Nernst-Einstein equation), so the convention is to plot  $\sigma T$  rather than  $\sigma$ , giving

$$\sigma T = A \exp\left(\frac{-E_a}{RT}\right), \quad (2)$$

Both equations can be linearised by taking logarithms, and it is common to plot the natural logarithm of  $D^*$  or  $\sigma T$  against inverse temperature, with this representation known as an “Arrhenius plot”. Data that approximate a straight line on an Arrhenius plot are said to exhibit “Arrhenius behaviour”.

While many systems show approximate Arrhenius behaviour, this is not universal. For some systems, Arrhenius plots show pronounced curvature, corresponding to “non-Arrhenius” behaviour that is not well-modelled by the Arrhenius equation. In these cases, alternative models—such as the Vogel-Tammann-Fulcher equation [9–13]—may provide a better description. However, it is not always clear whether observed deviations indicate genuine non-Arrhenius behaviour or simply reflect noise in the data, raising the question of how to determine which model is best supported by a given dataset.

Fitting an empirical model requires determining the values of its parameters, e.g., for the Arrhenius model, the activation energy  $E_a$  and pre-exponential factor  $A$ . Because the underlying data have scatter or associated uncertainties, we need not only best-fit parameter values but also the associated inverse uncertainties, the uncertainties in the fitted parameters inferred from the data.

Once a model has been fitted, a common use is to extrapolate to temperatures outside the measured range; for example, to predict room-temperature conductivity

\* andrew.mccluskey@bristol.ac.uk

† b.j.morgan@bath.ac.uk

from high-temperature simulation data [14, 15]. Such extrapolations assume the model remains valid in the new regime, and for the extrapolated estimates to be meaningful, the inverse uncertainties in the fitted parameters must be propagated correctly into the predicted values.

The challenges outlined above—obtaining fitted parameters with meaningful uncertainties, assessing which model is best supported by the data, and quantifying confidence in extrapolations—are non-trivial and often not addressed by standard fitting approaches. Bayesian methods provide a rigorous framework for addressing all three: they yield full probability distributions for fitted parameters, enable rational comparison of competing models, and allow uncertainty propagation into extrapolated predictions.

This tutorial details how to apply Bayesian methods to the analysis of temperature-dependent transport data. Our examples focus on conductivity estimates from molecular dynamics simulations of superionic materials, but the methodology is generally applicable wherever transport measurements have accurate uncertainty estimates. The methods outlined here are available in the open-source Python package KINISI [16].

## II. CHALLENGES IN TEMPERATURE-DEPENDENT MODELLING

Fitting empirical models to temperature-dependent transport data raises three significant challenges: selecting an appropriate model, determining parameter values with meaningful uncertainties, and extrapolating reliably to unmeasured temperatures. We examine each of these challenges below, before showing how Bayesian methods address them in Sections III–V.

### A. Model Selection

Given a set of temperature-dependent data, how do we determine which empirical model best describes the underlying behaviour? If we fit multiple candidate models and compare residuals, a more complex model with more free parameters will generally fit better than a simpler one, even when the additional complexity is not justified by the data. Using an overly complex model risks fitting noise rather than signal, producing parameter estimates that are precise but inaccurate, and extrapolations that are unreliable.

A model with more free parameters can fit a wider range of possible behaviours. If such a model fits the data, this is less informative than if a simpler, more constrained model fits equally well. The simpler model has made a more specific prediction that happened to be confirmed. When two models fit the data comparably, preferring the simpler model is not mere parsimony; it reflects the fact that the simpler model has been more

strongly tested. What we need is a framework that balances fit quality against model complexity. Simple tools, such as the Akaike and Bayesian information criteria, exist [17, 18], but they are based on assumptions, such as that the model parameters follow a normal distribution. Whereas, Bayesian model selection provides a robust approach to rationally compare different analytical models, and we discuss this in Section IV.

### B. Parameter Estimation

To fit a model to data, we must determine its parameter values. But given noisy or uncertain data, there is not a single set of parameters that is uniquely consistent with the observations—many different parameter combinations could plausibly describe the data we see. Rather than seeking a single “best fit”, we want a way to characterise the full set of parameter values that are compatible with our data. Standard fitting approaches return point estimates, perhaps with symmetric error bars that quantify spread around the best fit. But this representation is incomplete; it doesn’t capture the full range of models consistent with the data, nor any correlations or asymmetries in how parameters relate to one another. Bayesian posterior sampling provides a natural framework for this. Rather than returning a single parameter estimate, it generates samples from the distribution of parameter values that are compatible with the observed data. This posterior distribution fully characterises our uncertainty about the model parameters, as we discuss in Section III.

### C. Extrapolation

Once we have fitted a temperature-dependent model, a common goal is to predict behaviour at temperatures outside the measured range; for example, estimating room-temperature conductivity from high-temperature simulations [15]. For such extrapolations to be meaningful, the uncertainties in the fitted parameters must propagate into the extrapolated predictions. Without these, extrapolated values cannot be meaningfully compared to other values or assessed for reliability. Bayesian posterior sampling makes uncertainty propagation straightforward: the same parameter samples used to characterise the fit can be propagated through the model to generate a distribution of predicted values at any temperature, as we discuss in Section V.

## III. PARAMETER ESTIMATION

With the challenges outlined, we now turn to Bayesian methods for addressing them. Although model selection is conceptually prior (we need to decide which model to

fit), in practice, we must understand how to fit a single model before we can compare models. We therefore begin with parameter estimation. In this section, we assume the data follow the Arrhenius model and demonstrate how Bayesian posterior sampling yields parameter estimates with meaningful uncertainties. The approach is general, however, and applies to any parametric model.

As discussed in Section II, our goal is not to find a single “best” set of parameter values, but to characterise the full range of parameter values that are compatible with our data. For the Arrhenius model, this means finding all combinations of activation energy,  $E_a$ , and pre-exponential factor,  $A$ , that could plausibly describe the observed temperature-dependent conductivity.

Given a set of measured conductivities at different temperatures, how do we determine which parameter values are compatible with these data? The starting point is to ask: for a given choice of  $E_a$  and  $A$ , how well does the model predict the observed data? We quantify this using the likelihood: the probability of observing our data given a particular set of parameter values. This is a conditional probability, written  $p(\mathbf{x} | \theta)$ , where  $\mathbf{x}$  denotes our data and  $\theta$  the parameters. If a parameter combination produces model predictions that closely match the observations (within their uncertainties), the likelihood is high; if the predictions are far from the data, the likelihood is low.

The likelihood tells us how probable our data are given some parameters. But this is not quite what we want. We want the inverse: how probable are the parameters given our data? This is the posterior distribution, written  $p(\theta | \mathbf{x})$ . Likelihood and posterior are related but not the same:  $p(\mathbf{x} | \theta)$  is not the same as  $p(\theta | \mathbf{x})$ . The relationship between them is given by Bayes’ theorem:

$$p(\theta | \mathbf{x}) = \frac{p(\mathbf{x} | \theta) \times p(\theta)}{p(\mathbf{x})}. \quad (3)$$

Here,  $p(\theta | \mathbf{x})$  is the posterior: the probability of parameters  $\theta$  given the data.  $p(\mathbf{x} | \theta)$  is the likelihood.  $p(\theta)$  is the prior: our knowledge about plausible parameter values before seeing the data.  $p(\mathbf{x})$  is a normalising constant that ensures the posterior integrates to one. Because  $p(\mathbf{x})$  is a constant for any given dataset, the posterior is proportional to the likelihood times the prior:

$$p(\theta | \mathbf{x}) \propto p(\mathbf{x} | \theta) \times p(\theta). \quad (4)$$

This means we can characterise the posterior by evaluating the likelihood and prior across parameter space.

The prior distribution,  $p(\theta)$ , encodes what we know about plausible parameter values before examining the data. In many cases, we have little prior knowledge, in which case we use broad, minimally informative priors: for example, a uniform distribution over a physically reasonable range. For the Arrhenius model, we require  $E_a > 0$  (activation energies are positive) and  $A > 0$  (the pre-exponential factor is positive). Beyond these physical constraints, we might specify uniform priors over ranges

that comfortably encompass expected values. Provided the data are informative, the posterior will be dominated by the likelihood, so the precise choice of prior is often not critical; but it should always be reported.

For simple models with few parameters, we could evaluate the posterior on a fine grid across parameter space. But this becomes impractical as the number of parameters grows. Instead, we use sampling algorithms that explore parameter space efficiently, spending more time in regions of high posterior probability. Markov chain Monte Carlo (MCMC) is a widely used family of sampling algorithms. The details of how MCMC works are beyond the scope of this tutorial, but the essential idea is that it generates a sequence of parameter samples that, collectively, represent the posterior distribution. From these samples, we can compute summary statistics (means, medians, credible intervals) or visualise the full distribution.

To apply this framework, we need to specify the likelihood function. For temperature-dependent conductivity data, we assume that the measurement errors are normally distributed around the true values. This assumption is often reasonable on two grounds. First, the central limit theorem: if measurement errors arise from many independent sources, their sum will tend toward a normal distribution. Second, the principle of maximum entropy: if we know only the mean and variance of a distribution, the normal distribution is the one that assumes the least additional structure. If we know only the mean and variance of our errors, the normal distribution is the maximum-entropy choice. Any other distribution would imply structure we have no evidence for. With this assumption, the likelihood takes the form of a multivariate normal distribution:

$$p(\mathbf{x} | \theta) = (2\pi)^{-\frac{k}{2}} |\Sigma|^{-\frac{1}{2}} \exp \left\{ -\frac{1}{2} [\boldsymbol{\mu} - \mathbf{x}]^\top \Sigma^{-1} [\boldsymbol{\mu} - \mathbf{x}] \right\}, \quad (5)$$

where  $k$  is the number of measured temperatures,  $\boldsymbol{\mu}$  is a vector of the measured conductivity values,  $\Sigma$  is the covariance matrix of measurement uncertainties, and  $p(\mathbf{x} | \theta)$  is the model prediction for parameters  $\theta$ .

In practice, the procedure is as follows. We start with a model—here, the Arrhenius equation—and define priors for each parameter. We then construct the likelihood function using our measured data and their uncertainties. The sampler explores parameter space, evaluating the product of likelihood and prior at each point. Combinations that fit the data well and satisfy the prior receive high probability; those that fit poorly or lie outside the prior bounds receive low probability. After sufficient exploration, the collected samples represent the posterior distribution. From these samples, we can extract summary statistics (e.g., means, medians, credible intervals) or visualise the full distribution to understand correlations between parameters.

As an example of this procedure, we analyse lithium-ion conductivity data from molecular dynamics simulations of the cubic phase of lithium lanthanum zirconium oxide (c-LLZO), a solid electrolyte of interest for solid-

state batteries (see Appendix for the simulation details). The data come from simulations at four temperatures (500 K, 600 K, 700 K and 800 K), giving us four conductivity estimates with associated uncertainties. To sample the posterior, we need to specify priors for  $E_a$  and  $A$ . Since we have no strong prior knowledge, we use broad uniform distributions that comfortably span the range of physically plausible values. With the likelihood and priors defined, we can run the sampler. Full details of the prior ranges and sampling procedure are given in the Appendix.

The sampler returns a set of samples drawn from the joint posterior distribution  $p(E_a, A | \mathbf{x})$ . Each sample is a point in parameter space: a specific  $(E_a, A)$  combination that corresponds to a curve on the Arrhenius plot. Fig. 1(a) shows the data with many such curves overlaid: the shaded bands indicate where curves cluster more or less densely, reflecting which parameter combinations are more probable given the data. Panel (b) shows these samples as a two-dimensional distribution, revealing that the parameters are highly correlated: higher values of  $E_a$  tend to be associated with higher values of  $A$ . Panels (c) and (d) show the marginal distributions for each parameter, obtained by integrating the samples along each axis. This is equivalent to integrating the joint distribution over the other parameter, asking, for example, “what is the probability of this value of  $E_a$ , regardless of  $A$ ?”

The activation energy is approximately normally distributed, with mean and 95 % credible interval of  $(0.123 \pm 0.016)$  eV . The pre-exponential factor, however, is not normally distributed—it follows an approximately log-normal distribution. For this parameter, we report the median and 95 % credible interval:  $(2.652_{-0.689}^{+0.891}) \times 10^6 \text{cm}^2 \text{s}^{-1}$  . This illustrates one advantage of Bayesian posterior sampling: we obtain the full distribution of each parameter, rather than assuming normality. For  $A$ , reporting a symmetric confidence interval around the mean would misrepresent our uncertainty.

Arrhenius models are often fitted by taking logarithms and using linear regression in the transformed space, plotting  $\ln(\sigma T)$  versus  $1/T$  and fitting a straight line. This approach is convenient, but introduces bias: if the errors in  $\sigma T$  are normally distributed, transforming to log space makes them log-normally distributed, violating the assumptions of linear regression and yielding biased estimates for  $E_a$  and  $A$  [19]. Our choice of a multivariate normal likelihood above also assumes normally distributed errors, so we must work with the untransformed data to satisfy this assumption.

While this section has discussed Bayesian parameter estimation using the example of the Arrhenius model, the approach generalises to other models; we need only specify the model equation and appropriate priors. However, we have so far assumed that the Arrhenius model is the correct choice. In the next section, we address how to compare models and select the one best supported by the data.

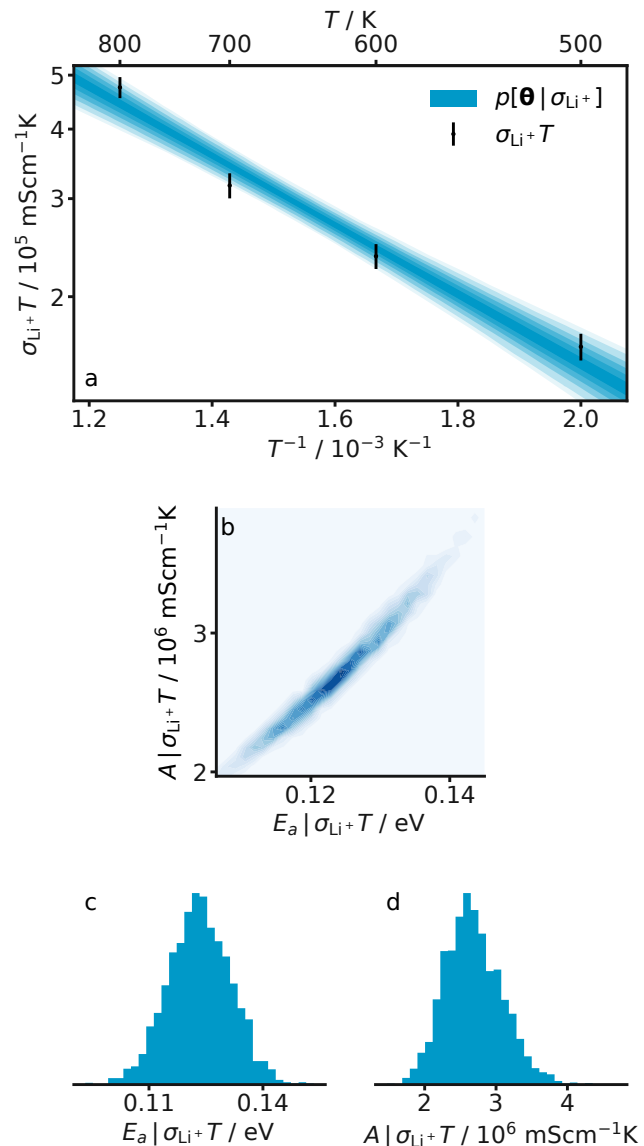


FIG. 1. (a) Lithium-ion conductivity in c-LLZO (black points; error bars show 95 % credible intervals). Blue curves show Arrhenius models evaluated using parameter samples drawn from the posterior; darker shading indicates where more curves overlap. (b) Joint posterior distribution showing the correlation between  $E_a$  and  $A$ . (c, d) Marginal posterior distributions for the activation energy and pre-exponential factor.

#### IV. MODEL SELECTION

In Section III, we assumed the data followed the Arrhenius model. But how do we know this is the right choice? As discussed in Section II, if we simply compare how well different models fit the data, a more complex model will generally fit better [20], even when the additional complexity is not justified. We need a rational approach that balances fit quality against model complexity. Bayesian model selection provides such a framework. Rather than

asking “which model fits best?”, it asks “which model is most probable given the data?”; and in answering this question, it naturally penalises unnecessary complexity.

To illustrate model selection, we compare the Arrhenius equation with the Vogel-Tammann-Fulcher (VTF) equation[10–12], an alternative model that allows the activation energy to vary with temperature. The VTF equation has the form:

$$\sigma T = A \exp \left[ \frac{-B}{R(T - T_0)} \right], \quad (6)$$

where  $A$  is the pre-exponential factor,  $B$  is related to the activation energy, and  $T_0$  is the Vogel temperature. The Arrhenius equation is a special case of VTF with  $T_0 = 0$ , so the VTF model will always fit the data at least as well as Arrhenius, because it has an additional parameter to adjust. The question is whether that additional parameter is justified by the data.

Given a dataset, how do we decide whether the additional parameter in the VTF model is justified by the data, or whether the simpler Arrhenius model is sufficient? The Bayesian approach is to ask which model is more probable given the data; that is, compute  $p(\text{model} | \mathbf{x})$ , or in more compact notation,  $p(m | \mathbf{x})$ . Applying Bayes’ theorem at the level of models rather than parameters:

$$p(m | \mathbf{x}) \propto p(\mathbf{x} | m) \times p(m). \quad (7)$$

Here,  $p(m)$  is our prior belief about the model before seeing the data. If we have no reason to prefer one model over another, we assign them equal prior probabilities. In that case, comparing posterior model probabilities reduces to comparing the marginal likelihood,  $p(\mathbf{x} | m)$ . The marginal likelihood is the probability of observing our data, averaged over all possible parameter values for that model. If we denote the parameters of model  $m$  as  $\theta_m$ , this is:

$$p(\mathbf{x} | m) = \int \cdots \int_{\theta_m} p(\mathbf{x} | \theta_m, m) p(\theta_m | m) d\theta_m. \quad (8)$$

The first term in the integral is the likelihood: how well parameters  $\theta_m$  predict the data. The second is the prior: how plausible those parameters are before seeing the data. This integral naturally penalises complex models. A model with more parameters spreads its prior probability over a larger parameter space. Unless the data actually constrain those extra parameters, much of this space will have low likelihood, dragging down the integral. A simpler model spreads its prior over a smaller space; if the data fall within this space, the integral is correspondingly larger. This connects to the intuition from Section II: a simpler model makes a more specific prediction. If that prediction is confirmed by the data, it provides stronger evidence than a flexible model that could have accommodated many different outcomes.

To compare two models, we compute the ratio of their marginal likelihoods:

$$B_{\beta\alpha} = \frac{p(\mathbf{x} | m_\beta)}{p(\mathbf{x} | m_\alpha)}. \quad (9)$$

This ratio is called the Bayes factor. If  $B > 1$ , the data favour model  $\beta$ ; if  $B_{\beta\alpha} < 1$ , they favour model  $\alpha$ . The magnitude indicates the strength of the evidence. A common interpretation, due to Kass and Raftery, is that  $\ln(B) > 5$  (corresponding to  $B > 150$ ) constitutes “very strong” evidence for the preferred model [21].

The integral for the marginal likelihood can be challenging to compute, particularly for models with many parameters. Markov chain Monte Carlo, which we used in Section III for parameter estimation, does not directly provide the marginal likelihood. Nested sampling is an alternative algorithm designed specifically for this purpose: it efficiently estimates the marginal likelihood while also providing posterior samples as a by-product. We do not detail the algorithm here, but point the reader to Sivia and Skilling for a pedagogical description [22].

As an example of Bayesian model selection, we compare the Arrhenius and VTF models using silver-ion conductivity data from molecular dynamics simulations of  $\text{AgCrSe}_2$  [9], a material previously reported to exhibit non-Arrhenius behaviour. The data span a range of temperatures and show apparent curvature in the Arrhenius plot; but do the data support a non-Arrhenius model, or is the simpler Arrhenius model sufficient?

We compute the Bayes factor comparing the VTF model ( $\beta$ ) to the Arrhenius model ( $\alpha$ ), assuming equal prior probabilities for each. Fig. 2 shows the results for two different simulation lengths. Panels (a) and (b) compare the Arrhenius and VTF fits using 40 ps of data from the diffusive regime [23]. Both models fit the data reasonably well, and the Bayes factor is  $\ln(B_{\beta\alpha}) = 1.3 \pm 0.3$ , where the uncertainty is a 95% confidence interval. This indicates weak evidence for the VTF model, but is well below the threshold for strong evidence. At this simulation length, we have no evidential basis for preferring the more complex VTF model.

Panels (c) and (d) show the same comparison using 140 ps of diffusive-regime data. The conductivity data appear similar, but the uncertainties are much smaller. With tighter error bars, the deviation from linearity becomes more clearly resolved. The Bayes factor increases to  $\ln(B_{\beta\alpha}) = 8.9 \pm 0.6$ , well above the threshold of 5, and strong evidence for the more complex VTF model over the simpler Arrhenius alternative.

Panel (e) shows how the Bayes factor evolves with simulation length. As the data become more precise, the evidence for non-Arrhenius behaviour grows. If the system were truly Arrhenius, longer simulations would not increase the Bayes factor, and we would continue to prefer the simpler model.

This example illustrates two points. First, Bayesian model selection tells us whether a more complex model is supported by the data or if we should prefer a simpler

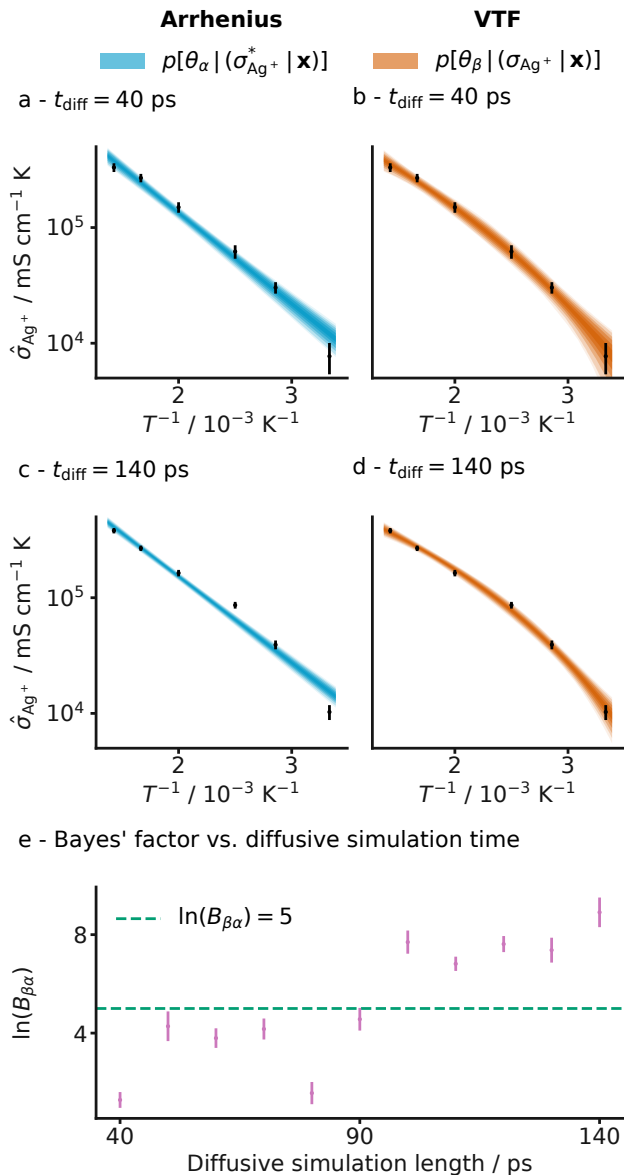


FIG. 2. Comparison of Arrhenius (a, c) and VTF (b, d) models for silver-ion conductivity in  $\text{AgCrSe}_2$ . Black points show conductivity estimates with 95% credible intervals. Coloured shading shows models evaluated at parameter values sampled from each posterior. Panels (a, b) use a fitting window of 40 ps; panels (c, d) use 140 ps. (e) Bayes factor comparing VTF to Arrhenius as a function of the amount of diffusive-regime data used,  $t_{\text{diff}}$ . The dashed line indicates  $\ln(B_{\beta\alpha}) = 5$ , the threshold for “very strong” evidence.

alternative. Second, it tells us whether our data are sufficient to answer the question we are asking. With 40 ps of simulation, we cannot confidently classify this behaviour as non-Arrhenius; with 140 ps, we can.

This section has demonstrated Bayesian model selection using the Bayes factor. The approach generalises to any set of competing models; we need only compute the marginal likelihood for each. In the next section, we ad-

dress the final challenge: extrapolating fitted models to temperatures outside the measured range.

## V. EXTRAPOLATION

In Sections III and IV, we fitted models to data within the measured temperature range. Often, however, we want to predict behaviour at temperatures outside this range: for example, estimating room-temperature conductivity from high-temperature simulations. As discussed in Section II, such extrapolations are only meaningful if the uncertainties in the fitted parameters propagate into the predicted values. A single extrapolated number without an associated uncertainty cannot be compared to other values or assessed for reliability.

Extrapolation amplifies parameter uncertainties. The Arrhenius equation is exponential: small changes in the activation energy produce large changes in predicted conductivity, particularly at temperatures far from the fitted range. If we report only a point estimate, e.g., using the “best fit” parameters to predict conductivity at a new temperature, we ignore this sensitivity and risk substantial overconfidence in the result.

Bayesian posterior sampling makes uncertainty propagation straightforward. In Section III, we obtained samples from the joint posterior distribution of parameters. Each sample represents a plausible  $(E_a, A)$  combination given the data. To extrapolate, we simply evaluate the model at the new temperature for each sample. The resulting collection of conductivity values represents the distribution of model predictions at that temperature; i.e., the range of conductivities compatible with our original data [24].

We demonstrate this using the LLZO posterior from Section III. Having sampled the joint distribution of  $E_a$  and  $A$  at temperatures between 500 K and 800 K, we now extrapolate to 300 K, well outside the original measurement range. For each posterior sample, we calculate  $\sigma(300 \text{ K})$  using the Arrhenius equation. The collection of these values gives us the distribution of predicted conductivities at room temperature.

Fig. 3 shows the result. The posterior distribution, shown as shaded bands in the main panel, widens substantially as we extrapolate to lower temperatures. The inset shows the distribution of predicted conductivity at 300 K. This distribution is broad and asymmetric, with a median and 95% credible interval of  $(75.1^{+30.2}_{-21.4}) \text{mS cm}^{-1}$ . The breadth of this distribution illustrates why uncertainty propagation matters. A point estimate at 300 K would suggest a precise prediction; the full distribution reveals that the extrapolated conductivity spans nearly an order of magnitude. This uncertainty is not a failure of the method; rather, it accurately reflects how much the data can tell us about behaviour at temperatures we did not measure.

A caveat: extrapolation assumes the fitted model remains valid at the new temperature. If the transport

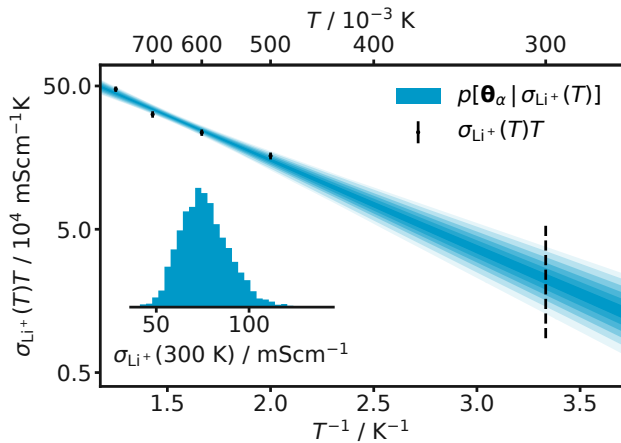


FIG. 3. Extrapolation of the LLZO conductivity model to 300 K (vertical dashed line). Blue shading shows Arrhenius models evaluated at parameter values sampled from the posterior (same data as Fig. 1). The shaded region widens at lower temperatures, reflecting increased uncertainty in the extrapolated predictions. Inset: distribution of predicted conductivity at 300 K.

mechanism changes, e.g., if a different diffusion pathway becomes dominant at lower temperatures, the extrapolation will be misleading regardless of how carefully we propagate uncertainty. Bayesian methods cannot verify this assumption; they can only tell us what to expect if the model holds.

This section has demonstrated how posterior samples enable straightforward extrapolation with uncertainty propagation. The same samples used to characterise the fit are simply evaluated at new temperatures, giving a distribution of predictions that reflects our uncertainty. Combined with parameter estimation (Section III) and model selection (Section IV), this completes the Bayesian framework for analysing temperature-dependent transport data.

## VI. CONCLUSIONS

This tutorial has introduced Bayesian methods for analysing temperature-dependent transport data, addressing three common challenges: estimating model parameters with meaningful uncertainties, selecting between competing models, and extrapolating predictions to unmeasured temperatures. For parameter estimation, Bayesian posterior sampling returns the full distribution of parameter values compatible with the data—capturing asymmetries and correlations that point estimates with symmetric error bars would miss. For model selection, Bayes factors provide a rational basis for choosing between models of different complexity. For extrapolation, the same posterior samples enable straightforward uncertainty propagation, revealing how much (or how little) the data constrain predictions outside the measured

range. The methods described here are implemented in the open-source Python package *kinisi* [16], which we hope will make Bayesian analysis of transport data more broadly accessible.

## METHODS

All conductivity data used in this work were derived from mean-squared displacement (MSD) analysis of molecular dynamics trajectories. Self-diffusion coefficients were estimated from the long-time slope of the MSD via the Einstein relation, using approximate Bayesian regression [25]. MSDs exhibit ballistic behaviour at short times and diffusive behaviour at longer times [26, 27]; only data from the diffusive regime, where the MSD is approximately linear in time, can be used for this fitting. Self-diffusion coefficients were converted to ionic conductivity estimates via the Nernst-Einstein relation, assuming a Haven ratio  $H_R = 1$ . All of the analysis in this work was performed with *KINISI-2.0.3* [16]. Analysis scripts are available in the Electronic Supplementary Information [28].

For  $\text{Li}_7\text{La}_3\text{Zr}_2\text{O}_{12}$  (LLZO), classical molecular dynamics simulations were run using the *METALWALLS* code [29]. The DIPPIM polarisable ion force field was used as parameterised by Burbano *et al.* [30]. The cubic phase of LLZO was simulated in the *NVT* ensemble at temperatures of 500 K, 600 K, 700 K and 800 K. Simulations were run for 50 ps using a 0.5 fs timestep and a Nosé-Hoover thermostat with a relaxation time of 121 fs [31–33]. The simulations used  $2 \times 2 \times 2$  supercells with 1536 atoms, following the same protocol as in Ref. 30. The simulation data are available under a CC BY 4.0 license on Zenodo [34].

The LLZO simulation trajectories were loaded into *KINISI* using the *MDANALYSIS* package [35, 36]. Mean-squared displacements of the lithium ions were computed at lag times from 0.5 fs to 50 ps in intervals of 2.5 fs. Self-diffusion coefficients were estimated with the start of the fitting window at 10 ps.

The LLZO conductivity data were modelled using the Arrhenius equation, using Markov chain Monte Carlo sampling. Parameter priors were uniform:  $p(E_a) \sim \mathcal{U}(0, 0.5 \text{ eV})$  and  $p(A) \sim \mathcal{U}(10^5, 10^7 \text{ cm}^2 \text{ s}^{-1})$ . The posterior distribution was sampled using 32 walkers, generating 10 000 samples after a burn-in period of 500 samples. Samples were thinned by a factor of 10 to reduce autocorrelation. For extrapolation, posterior samples were used to estimate conductivity at  $T = 300 \text{ K}$ .

For  $\text{AgCrSe}_2$ , simulation trajectories were provided by the authors of Ref. 9 as *lammprj* files. These simulations covered temperatures of 300 K, 350 K, 400 K, 500 K, 600 K and 700 K; full details are given in the original publication. The trajectories are available on Zenodo [37].  $\text{AgCrSe}_2$  simulation trajectories were loaded into *KINISI* using the *MDANALYSIS* package [35, 36] and mean-

TABLE I. MSD analysis parameters for AgCrSe<sub>2</sub>.  $\Delta t_{\min}$ : onset of diffusive regime, marking the beginning of the fitting window.  $\Delta(\Delta t)$ : spacing between successive lag times in the MSD computation.

$T / \text{K}$	$\Delta t_{\min} / \text{ps}$	$\Delta(\Delta t) / \text{ps}$
300	70.0	3.00
350	50.0	1.25
400	30.0	0.60
500	25.0	0.30
600	22.5	0.25
700	20.0	0.20

squared displacements computed at each temperature.

To investigate how the Bayes factor depends on data quality, we compared analyses using different fitting window lengths (from 40 ps to 140 ps, as shown in Fig. 2e).

The fitting window is the range of lag times used in the regression, starting from the onset of diffusive behaviour,  $\Delta t_{\min}$ . The start of the diffusive regime is temperature-dependent (Table I), so for a given fitting window length, the total trajectory length analysed varies with temperature. Mean-squared displacements were computed at lag times from  $\Delta t_{\min}$  to  $\Delta t_{\min}$  plus the fitting window length, in increments of  $\Delta(\Delta t)$  (Table I).

Bayesian model selection was performed using nested sampling [38] as implemented in the DYNESTY Python package [39], using 500 live points and a stopping criterion of 0.01. For the Arrhenius model, the parameter priors were:  $p(E_a) \sim \mathcal{U}(0, 1 \text{ eV})$  and  $p(A) \sim \mathcal{U}(10^4, 10^8 \text{ cm}^2 \text{ s}^{-1})$ . For the VTF model:  $p(B) \sim \mathcal{U}(0, 1 \text{ eV})$ ,  $p(A) \sim \mathcal{U}(10^4, 10^8 \text{ cm}^2 \text{ s}^{-1})$ , and  $p(T_0) \sim \mathcal{U}(0, 300 \text{ K})$ .

- 
- [1] Ohno, S. *et al.* Materials design of ionic conductors for solid state batteries. *Prog. in Energy* **2**, 022001 (2020).
- [2] Shah, A. R. *et al.* Neutron studies of Na-ion battery materials. *J. Phys.: Mater.* **4**, 042008 (2021).
- [3] Kumar, S. *et al.* Li-Ion Diffusion Correlations in LiAlGeO<sub>4</sub>: Quasielastic Neutron Scattering and Ab Initio Simulation. *ACS Appl. Energy Mater.* **5**, 14119–14126 (2022).
- [4] Eames, C. *et al.* Ionic transport in hybrid lead iodide perovskite solar cells. *Nat. Commun.* **6**, 7497 (2015).
- [5] Forrester, F. N., Quirk, J. A., Famprikis, T. & Dawson, J. A. Disentangling Cation and Anion Dynamics in Li<sub>3</sub>PS<sub>4</sub> Solid Electrolytes. *Chem. Mater.* **34**, 10561–10571 (2022).
- [6] Krenzer, G. *et al.* Nature of the Superionic Phase Transition of Lithium Nitride from Machine Learning Force Fields. *Chem. Mater.* **35**, 6133–6140 (2023).
- [7] Usler, A. L., Kemp, D., Bonkowski, A. & De Souza, R. A. A general expression for the statistical error in a diffusion coefficient obtained from a solid-state `jscp`/molecular-dynamics/`scpi` simulation. *J. Comput. Chem.* **44**, 1347–1359 (2023).
- [8] Canepa, P. Pushing Forward Simulation Techniques of Ion Transport in Ion Conductors for Energy Materials. *ACS Mater. Au* **3**, 75–82 (2022).
- [9] Wang, J., Ding, J., Delaire, O. & Arya, G. Atomistic Mechanisms Underlying Non-Arrhenius Ion Transport in Superionic Conductor AgCrSe<sub>2</sub>. *ACS Appl. Energy Mater.* **4**, 7157–7167 (2021).
- [10] Vogel, H. Das Temperaturabhaengigkeitsgesetz der Viskositaet von Fluessigkeiten. *Phys. Z.* **22**, 645 (1921).
- [11] Fulcher, G. S. Analysis of Recent Measurements of the Viscosity of Glasses. *J. Am. Ceram. Soc.* **8**, 339–355 (1925).
- [12] Tammann, G. & Hesse, W. Die Abhängigkeit der Viscosität von der Temperatur bie unterkühlten Flüssigkeiten. *Z. Anorg. Allg. Chem.* **156**, 245–257 (1926).
- [13] de Souza, V. K. & Wales, D. J. Super-Arrhenius Diffusion in an Undercooled Binary Lennard-Jones Liquid Results from a Quantifiable Correlation Effect. *Phys. Rev. Lett.* **96**, 057802 (2006).
- [14] Yeandel, S. R., Scanlon, D. O. & Goddard, P. Enhanced Li-ion dynamics in trivalently doped lithium phosphidosilicate Li<sub>2</sub>SiP<sub>2</sub>: a candidate material as a solid Li electrolyte. *J. Mater. Chem. A* **7**, 3953–3961 (2019).
- [15] Goldmann, B. A. *et al.* Rotational stacking faults in the ionic conductor Li<sub>3</sub>ScCl<sub>6</sub>. *Chem. Mater.* (2025).
- [16] McCluskey, A. R., Squires, A. G., Dunn, J., Coles, S. W. & Morgan, B. J. kinisi: Bayesian analysis of mass transport from molecular dynamics simulations. *J. Open Source Softw.* **9**, 5984 (2024).
- [17] Akaike, H. A new look at the statistical model identification. *IEEE Trans. Autom. Contr.* **19**, 716–723 (1974).
- [18] Schwarz, G. Estimating the Dimension of a Model. *Ann. Stat.* **6**, 461–464 (1978).
- [19] McCluskey, A. R. Is There Still a Place for Linearization in the Chemistry Curriculum? *J. Chem. Educ.* **100**, 4174–4176 (2023).
- [20] Mayer, J., Khairy, K. & Howard, J. Drawing an elephant with four complex parameters. *Am. J. Phys.* **78**, 648–649 (2010).
- [21] Kass, R. E. & Raftery, A. E. Bayes Factors. *J. Am. Stat. Assoc.* **90**, 773–795 (1995).
- [22] Sivia, D. S. & Skilling, J. *Data Analysis: A Bayesian Tutorial* (Oxford University Press, Oxford, UK, 2006), 2nd edn.
- [23] Mean-squared displacements exhibit ballistic behaviour at short times and diffusive behaviour at longer times [26, 27]. Because diffusion coefficients are estimated by linear regression of MSD against time, only data from the diffusive regime, where the MSD is approximately linear in time, is used for fitting.
- [24] This extrapolated distribution captures parameter uncertainty but not estimated measurement noise. For extrapolation far from the measured range, parameter uncertainty typically dominates, so this distinction is rarely important in practice.
- [25] McCluskey, A. R., Coles, S. W. & Morgan, B. J. Accurate Estimation of Diffusion Coefficients and their Un-

- certainties from Computer Simulation. *J. Chem. Theory Comput.* **21**, 79–87 (2024).
- [26] He, X., Zhu, Y., Epstein, A. & Mo, Y. Statistical variances of diffusional properties from ab initio molecular dynamics simulations. *npj Comput. Mater.* **4**, 18 (2018).
- [27] Bonkowski, A. & De Souza, R. A. From setup to analysis: A compact guide to performing Molecular Dynamics simulations of ion transport in solids. *Solid State Ionics* **429**, 116967 (2025).
- [28] McCluskey, A. R., Coles, S. W. & Morgan, B. J. model-arrhenius-0.0.1. <https://github.com/scams-research/model-arrhenius> (2025).
- [29] Marin-Lafèche, A. *et al.* MetalWalls: A classical molecular dynamics software dedicated to the simulation of electrochemical systems. *J. Open Source Softw.* **5**, 2373 (2020).
- [30] Burbano, M., Carlier, D., Boucher, F., Morgan, B. J. & Salanne, M. Sparse Cyclic Excitations Explain the Low Ionic Conductivity of Stoichiometric  $\text{Li}_7\text{La}_3\text{Xr}_2\text{O}_{12}$ . *Phys. Rev. Lett.* **116**, 135901 (2016).
- [31] Nosé, S. A unified formulation of the constant temperature molecular dynamics methods. *J. Chem. Phys.* **81**, 511–519 (1984).
- [32] Hoover, W. G. Canonical dynamics: Equilibrium phase-space distributions. *Phys. Rev. A* **31**, 1695–1697 (1985).
- [33] Martyna, G. J., Klein, M. L. & Tuckerman, M. Nosé–Hoover chains: The canonical ensemble via continuous dynamics. *J. Chem. Phys.* **97**, 2635–2643 (1992).
- [34] Coles, S. W. LLZO Simulation Trajectories. <https://doi.org/10.5281/zenodo.17702491> (2025).
- [35] Michaud-Agrawal, N., Denning, E. J., Woolf, T. B. & Beckstein, O. MDAnalysis: A toolkit for the analysis of molecular dynamics simulations. *J. Comput. Chem.* **32**, 2319–2327 (2011).
- [36] Gowers, R. *et al.* MDAnalysis: A Python Package for the Rapid Analysis of Molecular Dynamics Simulations. In *Proceedings of the 15th Python in Science Conference*, 98–105 (2016).
- [37] Wang, J., Ding, J., Delaire, O. & Arya, G. AgCrSe2 Simulation Trajectories. <https://doi.org/10.5281/zenodo.17910336> (2025).
- [38] Skilling, J. Nested Sampling. In *AIP Conference Proceedings*, vol. 735, 395–405 (AIP, 2004).
- [39] Speagle, J. S. dynesty: a dynamic nested sampling package for estimating bayesian posteriors and evidences. *Mon. Not. R. Astron. Soc.* **493**, 3132–3158 (2020).

# Supplemental Material for “Bayesian Methods for the Investigation of Temperature-Dependence in Conductivity”

Andrew R. McCluskey,<sup>1,2,\*</sup> Samuel W. Coles,<sup>3,4</sup> and Benjamin J. Morgan<sup>5,6</sup>

<sup>1</sup>*Centre for Computational Chemistry, School of Chemistry,  
University of Bristol, Cantock’s Close, Bristol, BS8 1TS, UK.*

<sup>2</sup>*Diamond Light Source, Harwell Campus, Didcot, OX11 0DE, UK.*

<sup>3</sup>*Yusuf Hamied Department of Chemistry, University of Cambridge, Lensfield Road, Cambridge, CB2 1EW, UK.*

<sup>4</sup>*Lennard-Jones Centre, University of Cambridge, Trinity Lane, Cambridge, CB2 1TN, UK.*

<sup>5</sup>*Department of Chemistry, University of Bath, Claverton Down, Bath, BA2 7AY, UK.*

<sup>6</sup>*The Faraday Institution, Quad One, Harwell Science and Innovation Campus, Didcot, OX11 0RA, UK.*<sup>†</sup>

This document presents supplementary material for the manuscript “Bayesian Methods for the Investigation of Temperature-Dependence in Conductivity”. It contains the following sections:

SI.I. Plots showing the mean-squared displacement and resulting linear model posterior distributions as a function of temperature for the LLZO systems.

SI.II. Plots showing the mean-squared displacement as a function of temperature, posterior distributions for  $\sigma$ , and the resulting Arrhenius, VTF models and distributions for  $E_a$  for a series of different amounts of diffusive simulation time for AgCrSe<sub>2</sub>.

A repository containing the analysis and plotting code used to generate all results and figures in the main manuscript and this supplemental material document is available at [www.github.com/arm61/model-arrhenius](https://www.github.com/arm61/model-arrhenius) [28], under MIT (code) and CC BY-SA 4.0 (figures and text) licenses. This repository includes a fully reproducible SHOWYOURWORK workflow, which allows complete reproduction of the analysis, plotting of figures and compilation of the manuscript.

## SI.I: Mean-squared displacement of LLZO as a function of temperature

Fig. SI.1 presents the mean-squared displacement data and resulting posterior distribution of linear models for a range of temperatures for LLZO. The marginal posterior distribution for  $D^*$  is then used to find  $\sigma$ , which is included in the LLZO analysis in the main text (??, Fig. 1, and Fig. 3).

## SI.II: Temperature dependence as a function of diffusive simulation time for AgCrSe<sub>2</sub>

Figs. SI.2 to SI.12 show the mean-squared displacement as a function of time interval for temperatures of 300 K, 350 K, 400 K, 500 K, 600 K and 700 K, where increasing total simulation lengths are used. Increasing the total simulation length has the effect of increasing the amount of diffusive simulation that is available in the analysis. As discussed in Sec. IV, this results in a large Bayesian evidence for the more complex VTF model.

---

\* [andrew.mccluskey@bristol.ac.uk](mailto:andrew.mccluskey@bristol.ac.uk)

<sup>†</sup> [b.j.morgan@bath.ac.uk](mailto:b.j.morgan@bath.ac.uk)

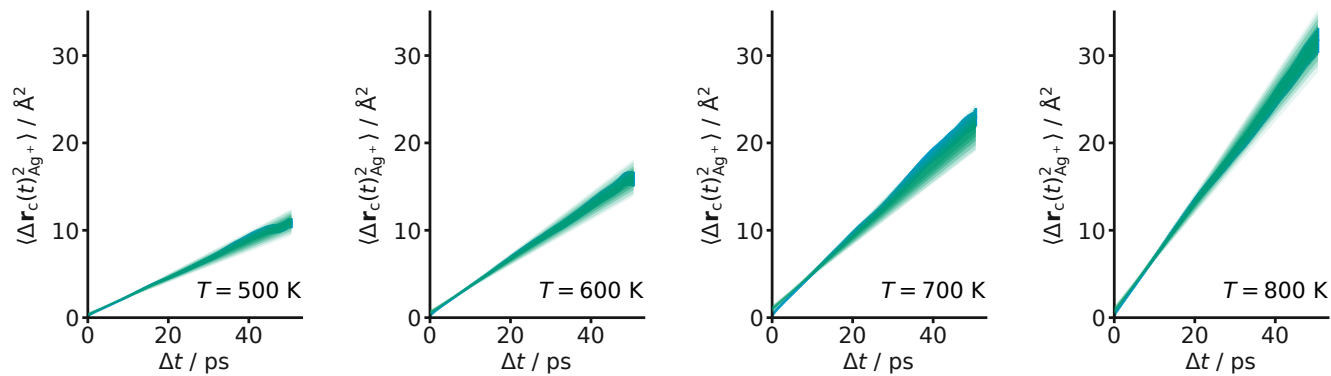


FIG. SI.1. The mean squared displacement data and associated distribution of linear models at temperatures of 500 K, 600 K, 700 K and 800 K with 50 ps of LLZO simulation.



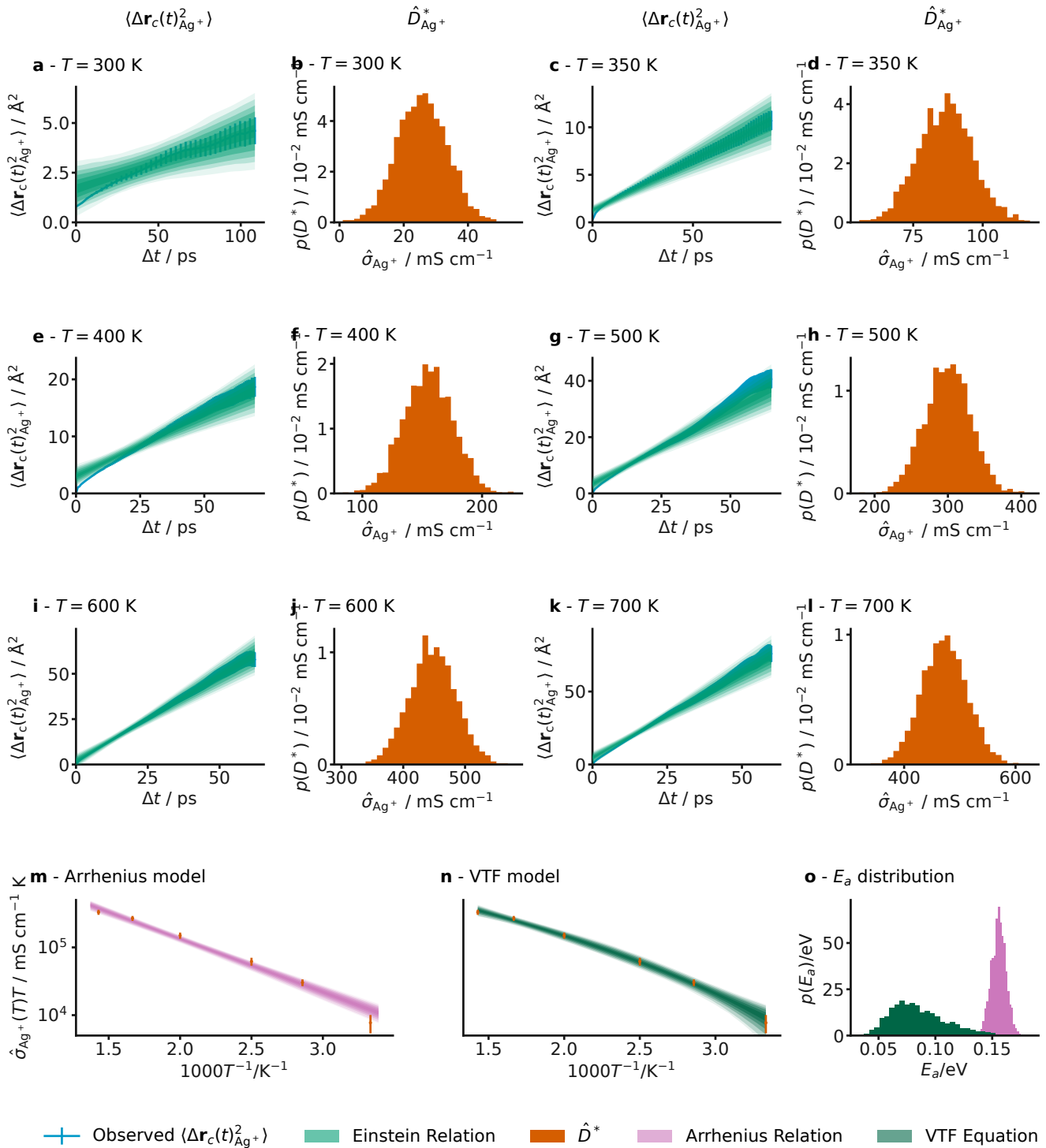


FIG. SI.2. The mean squared displacement data and associated  $\sigma$  distributions at temperatures of 300 K, 350 K, 400 K, 500 K, 600 K and 700 K with 40 ps of diffusive simulation (a-l), the appropriate Arrhenius (m) and VTF model (n) plots and the resulting distributions of  $E_a$  from each modelling approach (o).



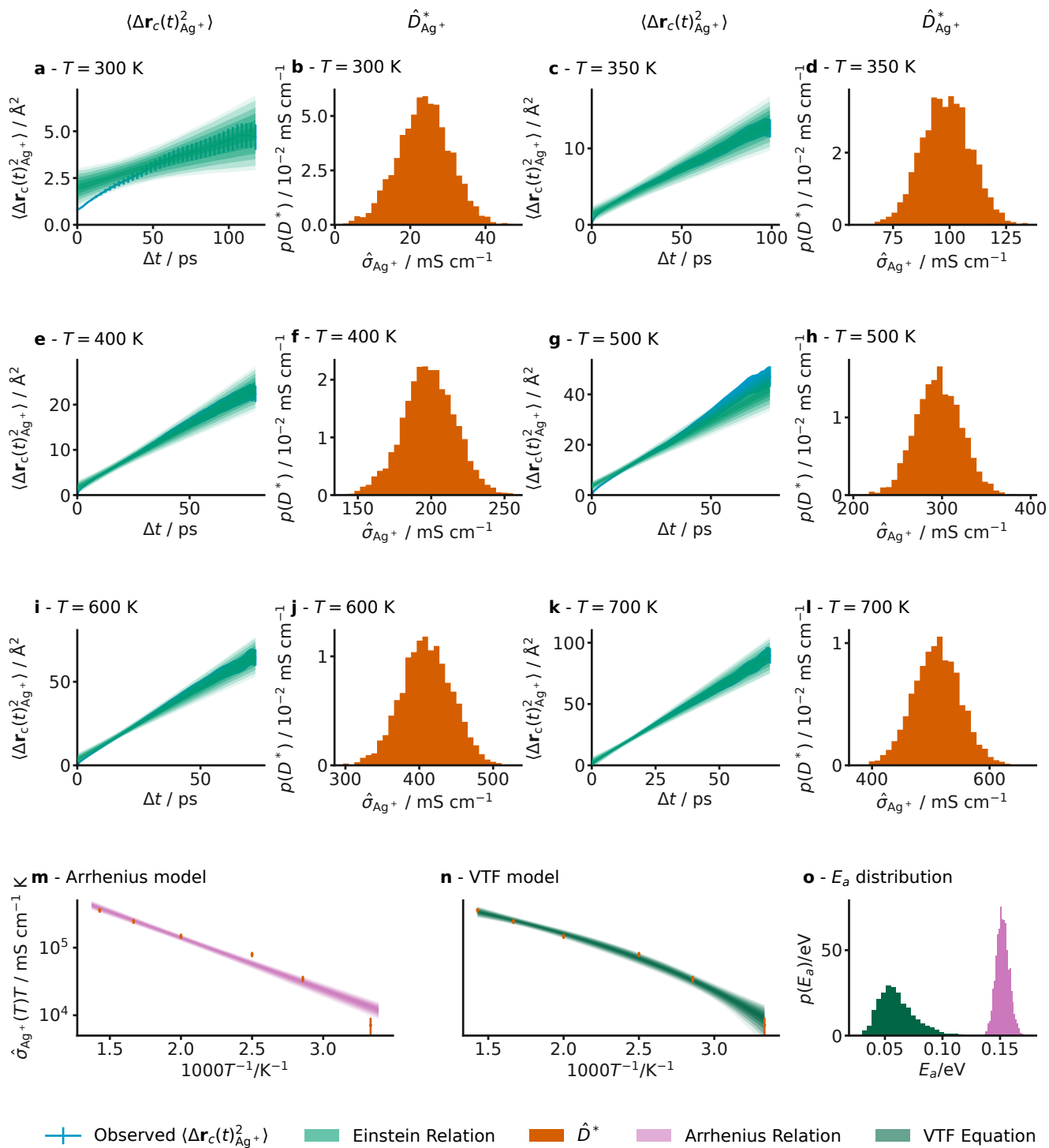


FIG. SI.3. The mean squared displacement data and associated  $\sigma$  distributions at temperatures of 300 K, 350 K, 400 K, 500 K, 600 K and 700 K with 120 ps of diffusive simulation (a-l), the appropriate Arrhenius (m) and VTF model (n) plots and the resulting distributions of  $E_a$  from each modelling approach (o).

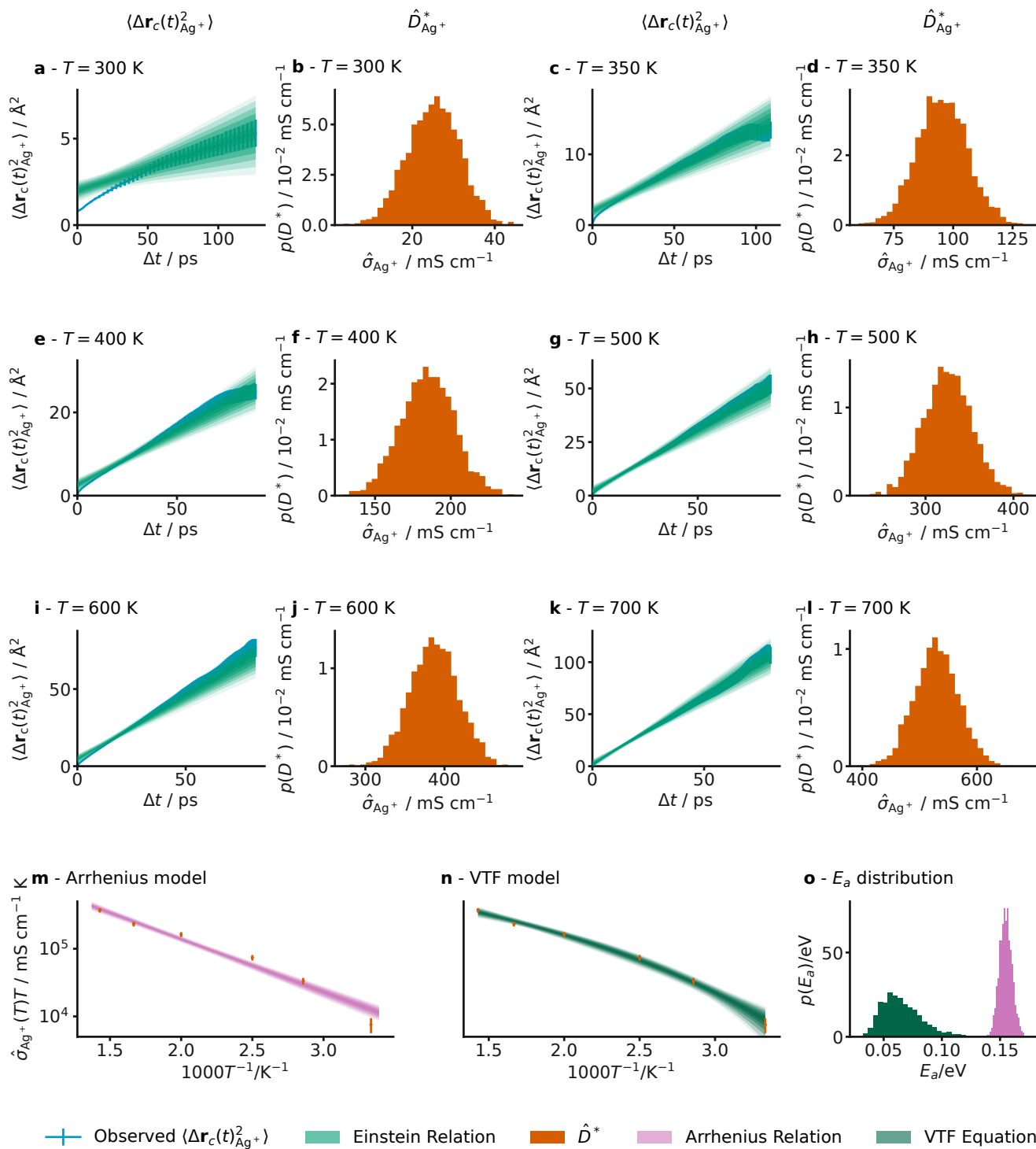


FIG. SI.4. The mean squared displacement data and associated  $\sigma$  distributions at temperatures of 300 K, 350 K, 400 K, 500 K, 600 K and 700 K with 60 ps of diffusive simulation (a-l), the appropriate Arrhenius (m) and VTF model (n) plots and the resulting distributions of  $E_a$  from each modelling approach (o).

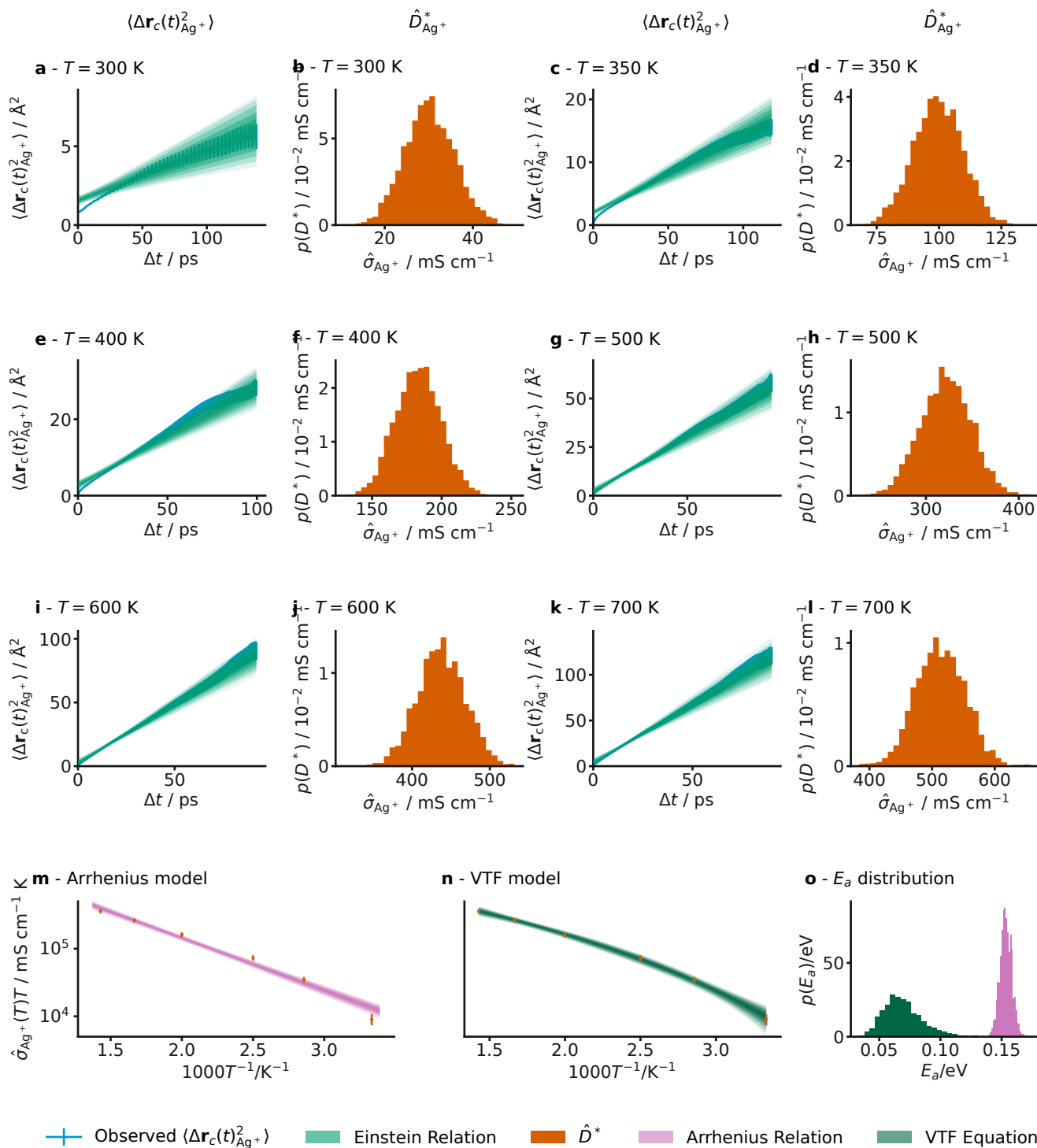


FIG. SI.5. The mean squared displacement data and associated  $\sigma$  distributions at temperatures of 300 K, 350 K, 400 K, 500 K, 600 K and 700 K with 120 ps of diffusive simulation (a-l), the appropriate Arrhenius (m) and VTF model (n) plots and the resulting distributions of  $E_a$  from each modelling approach (o).

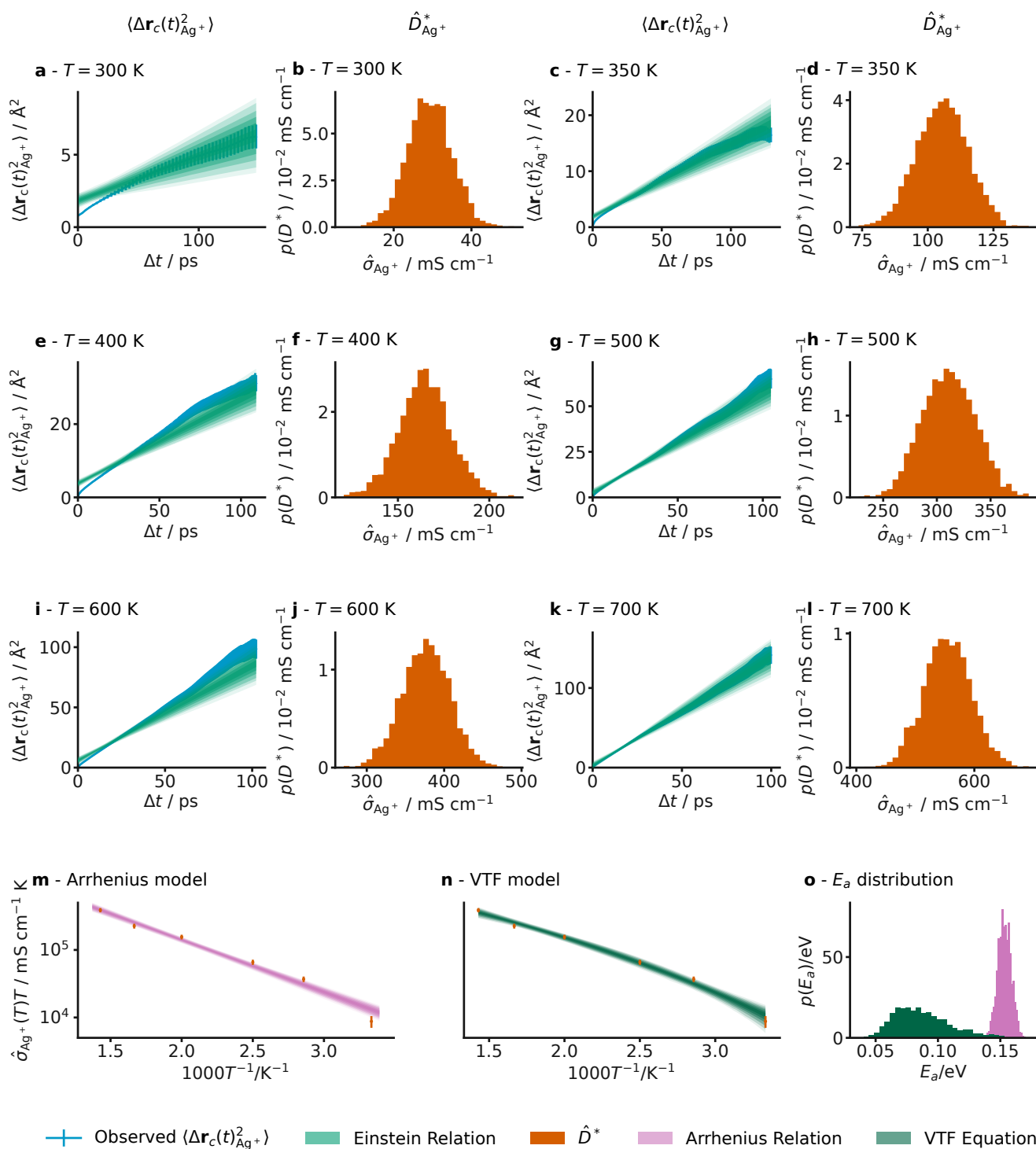


FIG. SI.6. The mean squared displacement data and associated  $\sigma$  distributions at temperatures of 300 K, 350 K, 400 K, 500 K, 600 K and 700 K with 80 ps of diffusive simulation (a-l), the appropriate Arrhenius (m) and VTF model (n) plots and the resulting distributions of  $E_a$  from each modelling approach (o).

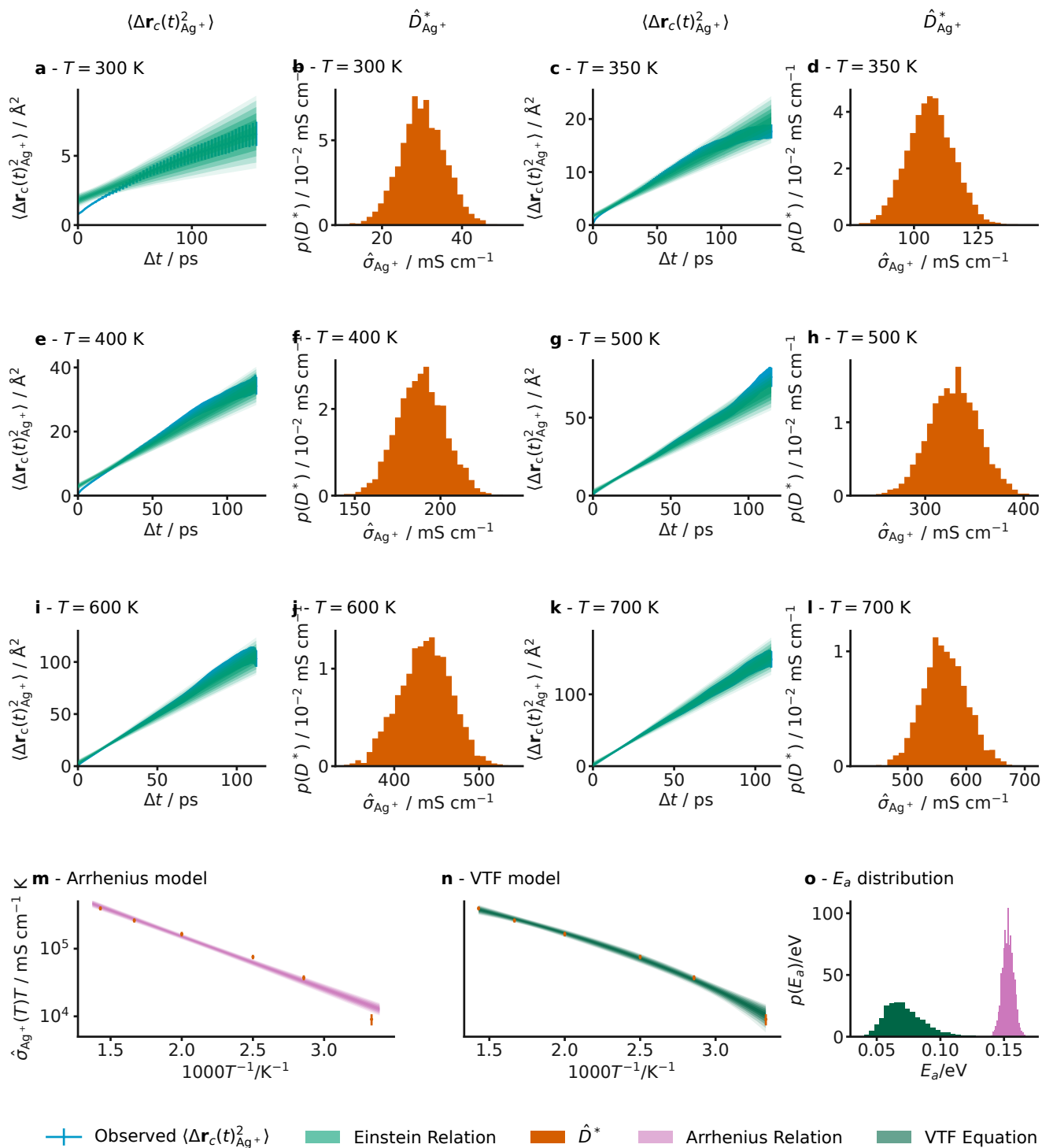


FIG. SI.7. The mean squared displacement data and associated  $\sigma$  distributions at temperatures of 300 K, 350 K, 400 K, 500 K, 600 K and 700 K with 120 ps of diffusive simulation (a-l), the appropriate Arrhenius (m) and VTF model (n) plots and the resulting distributions of  $E_a$  from each modelling approach (o).

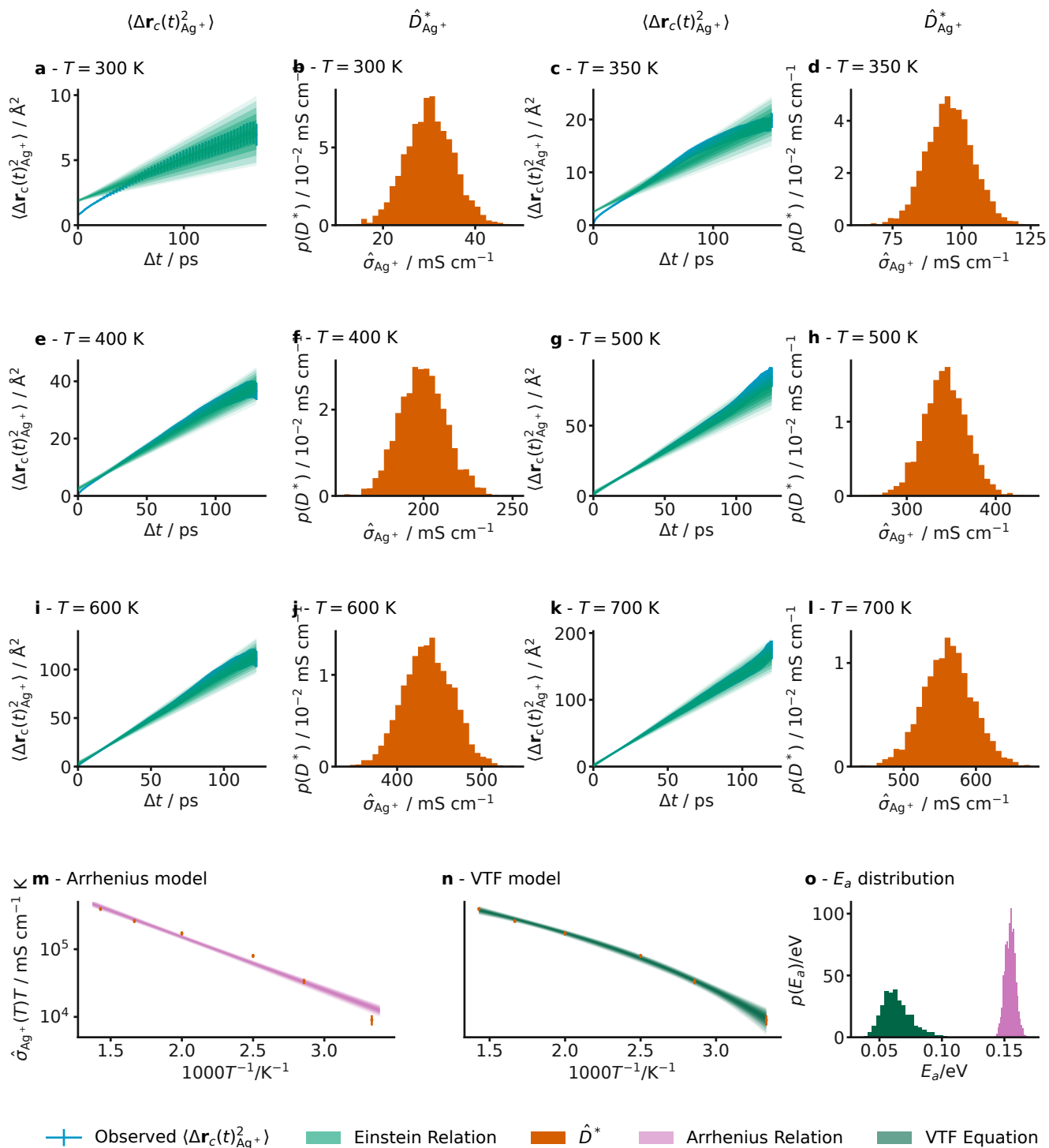


FIG. SI.8. The mean squared displacement data and associated  $\sigma$  distributions at temperatures of 300 K, 350 K, 400 K, 500 K, 600 K and 700 K with 100 ps of diffusive simulation (a-l), the appropriate Arrhenius (m) and VTF model (n) plots and the resulting distributions of  $E_a$  from each modelling approach (o).

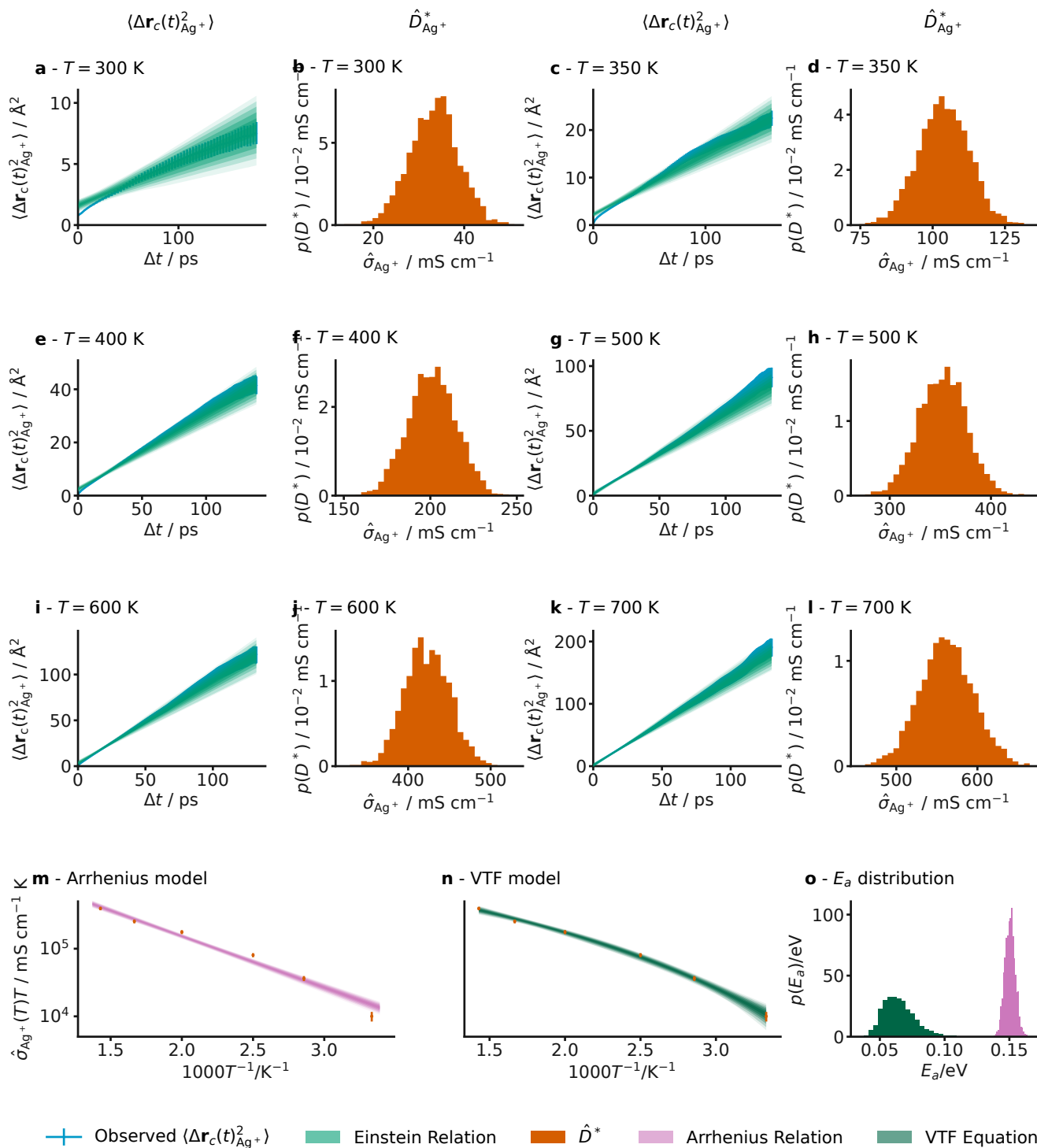


FIG. SI.9. The mean squared displacement data and associated  $\sigma$  distributions at temperatures of 300 K, 350 K, 400 K, 500 K, 600 K and 700 K with 120 ps of diffusive simulation (a-l), the appropriate Arrhenius (m) and VTF model (n) plots and the resulting distributions of  $E_a$  from each modelling approach (o).

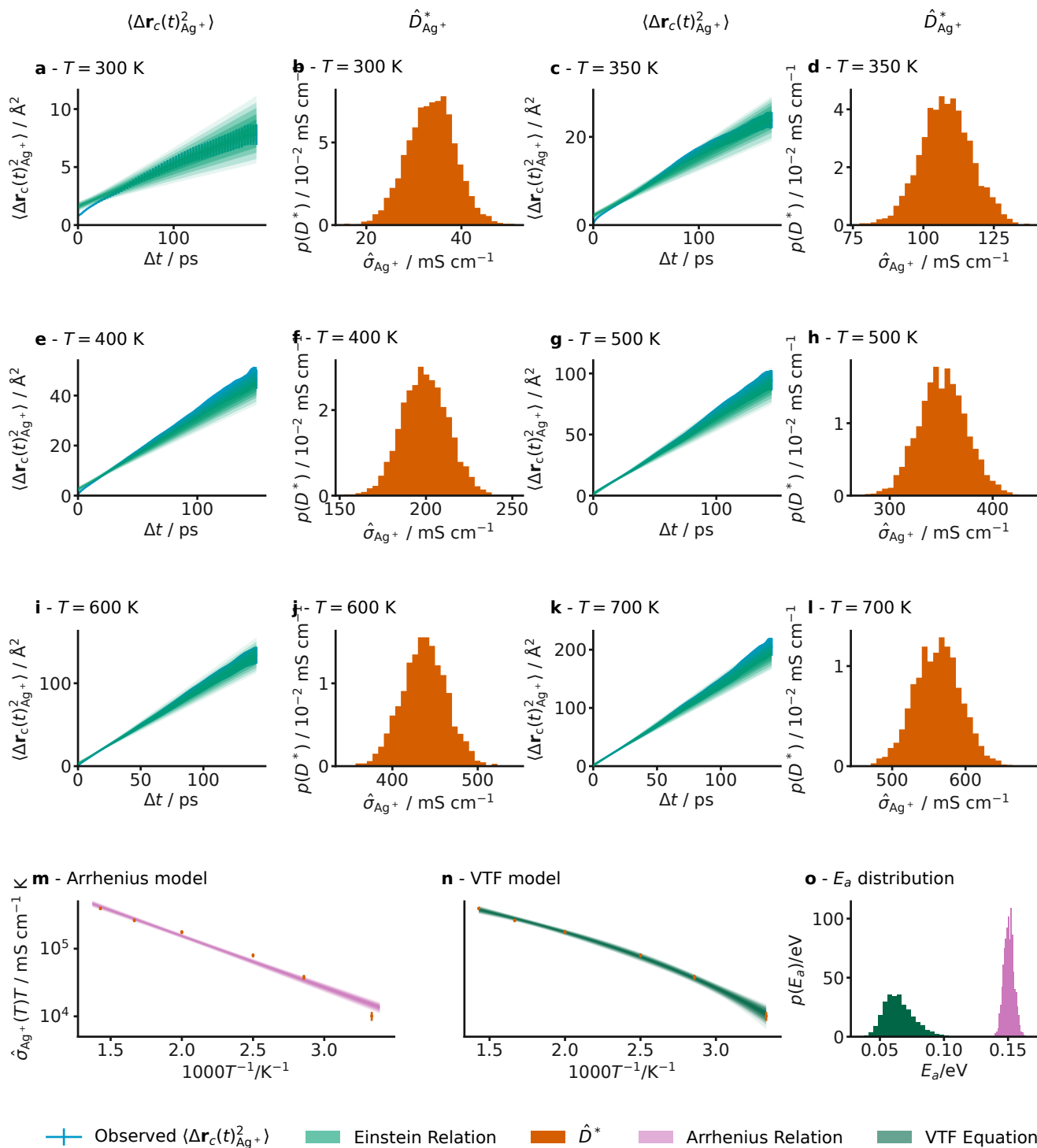


FIG. SI.10. The mean squared displacement data and associated  $\sigma$  distributions at temperatures of 300 K, 350 K, 400 K, 500 K, 600 K and 700 K with 120 ps of diffusive simulation (a-l), the appropriate Arrhenius (m) and VTF model (n) plots and the resulting distributions of  $E_a$  from each modelling approach (o).

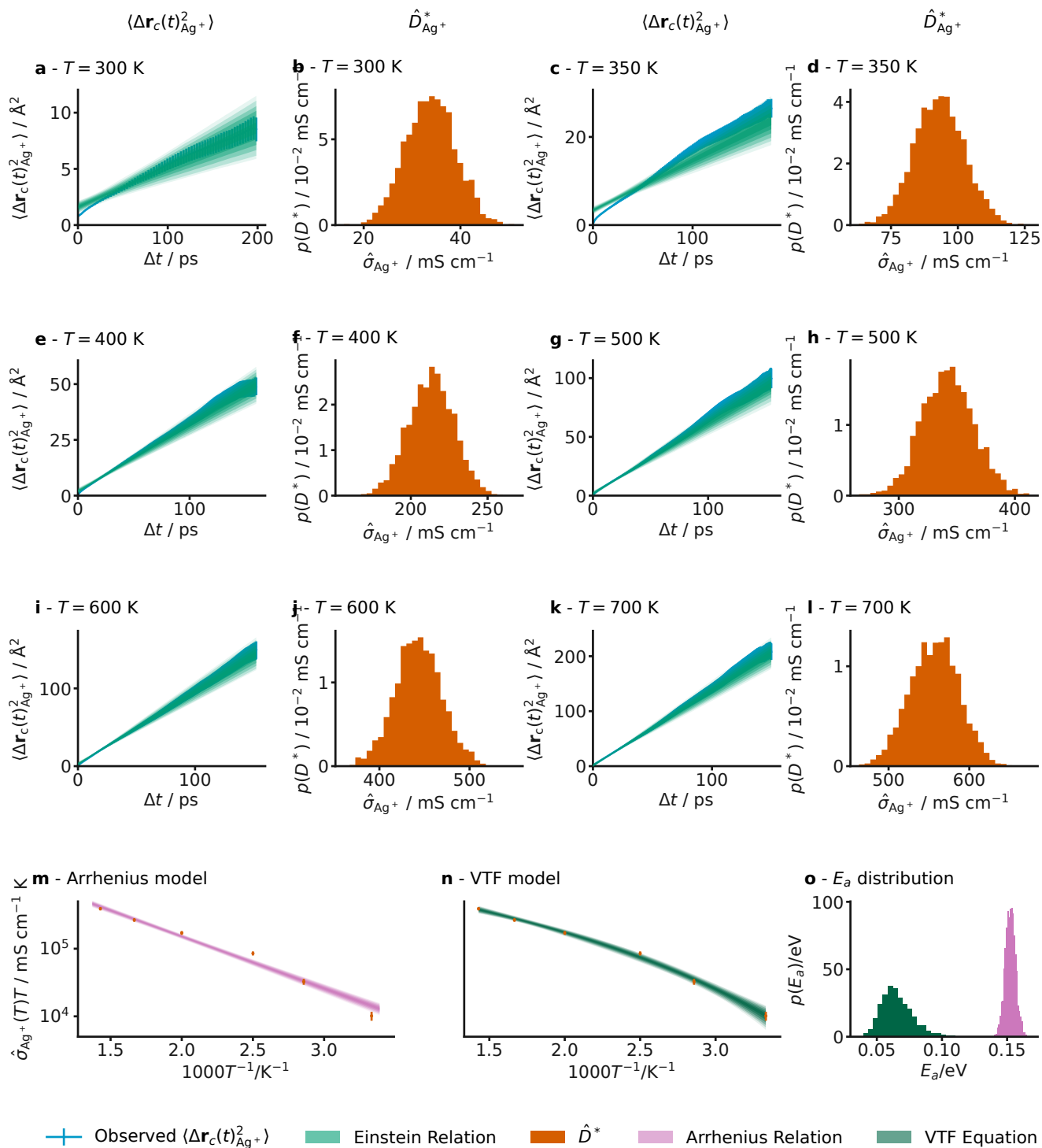


FIG. SI.11. The mean squared displacement data and associated  $\sigma$  distributions at temperatures of 300 K, 350 K, 400 K, 500 K, 600 K and 700 K with 120 ps of diffusive simulation (a-l), the appropriate Arrhenius (m) and VTF model (n) plots and the resulting distributions of  $E_a$  from each modelling approach (o).

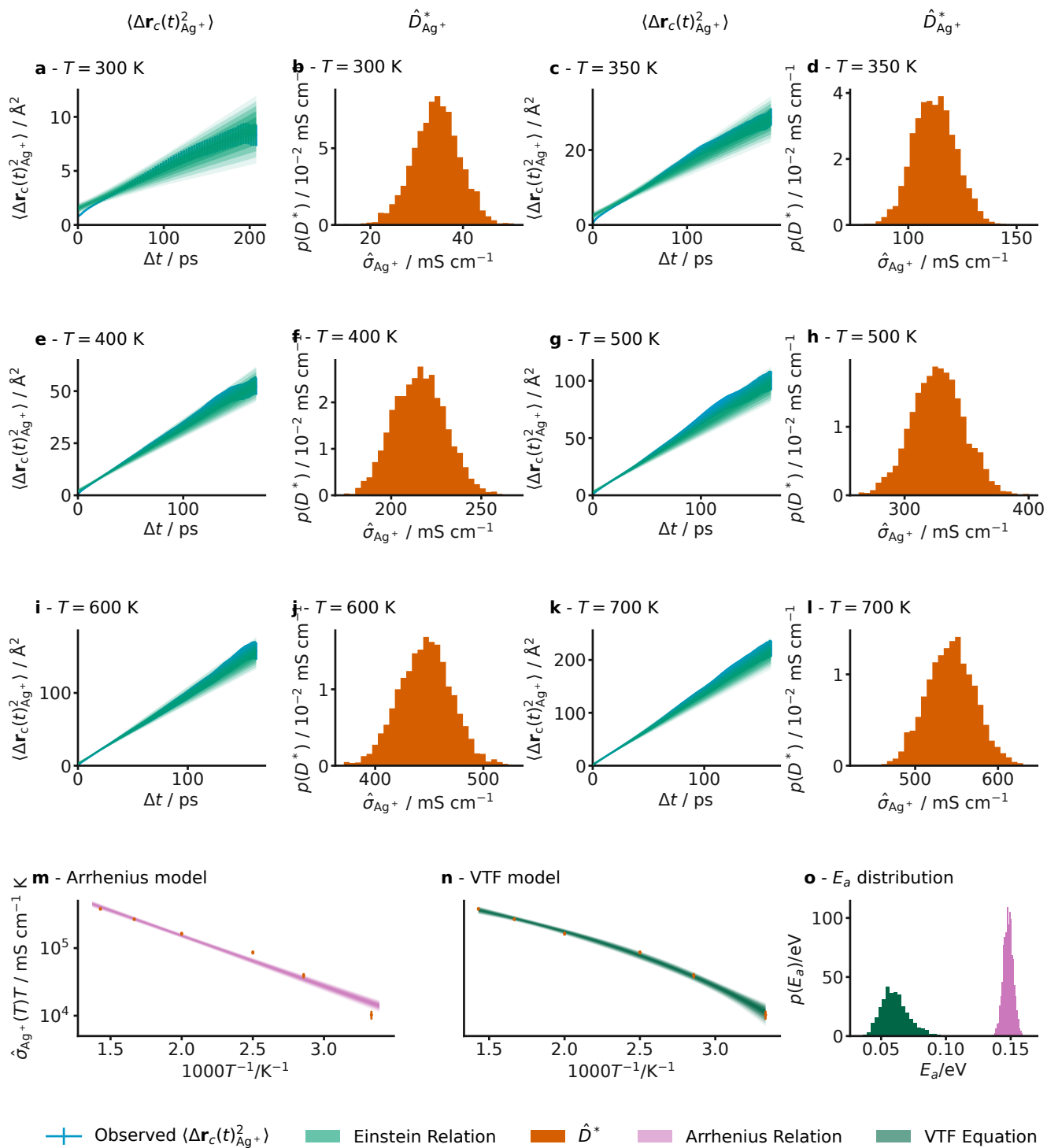


FIG. SI.12. The mean squared displacement data and associated  $\sigma$  distributions at temperatures of 300 K, 350 K, 400 K, 500 K, 600 K and 700 K with 140 ps of diffusive simulation (a-l), the appropriate Arrhenius (m) and VTF model (n) plots and the resulting distributions of  $E_a$  from each modelling approach (o).